Available online at www.sciencedirect.com
SCIENCE DIRECT®
Journal of Nuclear Materials 346 (2005) 233–243
journal of nuclear materials
www.elsevier.com/locate/jnucmat

Radiation embrittlement behavior of fine-grained molybdenum alloy with 0.2 wt%TiC addition

Y. Kitsunai [a,1], H. Kurishita [b,*], T. Kuwabara [a,2], M. Narui [b], M. Hasegawa [b], T. Takida [c], K. Takebe [c]

[a] *Tohoku University, Japan*
[b] *International Research Center for Nuclear Materials Science, Institute for Materials research (IMR), Tohoku University, Oarai, Ibaraki 311-1313, Japan*
[c] *A.L.M.T. TECH Inc., 2 Iwasekoshi-machi, Toyama 931-8543, Japan*

Received 22 April 2005; accepted 19 June 2005

Abstract

In order to elucidate the effects of pre-irradiation microstructures and irradiation conditions on radiation embrittlement and radiation-induced ductilization (RIDU), fine-grained Mo–0.2 wt%TiC specimens with high and low reduction rates in plastic working, which are designated as MTC-02H and MTC-02L, respectively, were prepared by powder metallurgical methods. The specimens were neutron irradiated to 0.1–0.15 dpa with controlled 1-cycle and 4-cycle heating between 573 and 773 K, and 473 and 673 K, respectively, in JMTR. Vickers microhardness and three-point bending impact tests and TEM microstructural examinations were made. The degree of radiation embrittlement, assessed by DBTT shift due to irradiation, was strongly dependent on the reduction rate and cycle number. The 4-cycle irradiation suppressed the radiation embrittlement compared with the 1-cycle irradiation, and the suppression was much more significant in MTC-02L than in MTC-02H. The observed behavior is discussed in connection with RIDU and microstructural evolution caused by the 4-cycle irradiation.

PACS: 28.52.Fa; 62.20.Mk

1. Introduction

Molybdenum (Mo) and its alloys are candidate materials for use as high-heat-flux-components because of its high melting point, high thermal conductivity, low sputtering yields, etc. However, they exhibit serious embrittlement by high-energy particle irradiation even with a low-level exposure [1–24]. It is therefore required to develop Mo alloys with improved resistance to radiation embrittlement.

* Corresponding author. Tel.: +81 29 267 4157; fax: +81 29 267 4947.
E-mail address: kurishi@imr.tohoku.ac.jp (H. Kurishita).
[1] Present address: Nippon Nuclear Fuel Development Co. Ltd. Oarai, Ibaraki 311-1313, Japan.
[2] Present address: Electronics & Materials R&D Laboratories, Sumitomo Electric Industries, Ltd., Osaka Works, 1-1-3, Shimaya, Konohana-ku, Osaka 554-0024, Japan.

0022-3115/$ - see front matter © 2005 Elsevier B.V. All rights reserved.
doi:10.1016/j.jnucmat.2005.06.013

It has been believed that radiation embrittlement arises from radiation hardening and thus inevitably occurs since irradiation always causes hardening except for high temperature irradiation, where appreciable recovery of an irradiation-induced microstructure may occur and result in a less degree of radiation hardening or even softening. Radiation hardening is mainly due to irradiation-produced defects and therefore it has been long believed that the only way to relieve radiation embrittlemnet is to suppress radiation hardening by introducing a large number of sink sites for irradiation-produced defects. Recent progress in both the development of irradiation rigs and materials fabrication techniques has been able to alter this consequence of radiation embrittlement. In 1996, the authors found that the low-temperature ductility of a TiC dispersed Mo alloy (Mo–1.0 wt%TiC, designated as MTC-10A) increased significantly by fast neutron irradiation to 0.08 dpa under controlled heat cycles between 573 and 773 K with 5 cycles in the Japan Materials Testing Reactor (JMTR); approximately five times as measured with three-point bending (3PB) impact tests, in spite of significant radiation hardening [25]. This ductility increase due to irradiation is entirely opposite to radiation embrittlement and is regarded as radiation-induced ductilization (RIDU) [26,27].

The only possible explanation for the occurrence of RIDU is as follows: most of materials contain microstructural inhomogeneities including grain boundaries and interfaces acting as crack initiation and/or propagation sites and such weak portions are strengthened (i.e., become more resistant to fracture) by irradiation, where the beneficial effect exceeds the detrimental effect of radiation hardening. The weak portion in Mo is well known to be grain boundaries with high energy [28–30]. Therefore, the RIDU observed in MTC-10A was attributed to strengthening of weak grain boundaries by radiation-enhanced precipitation and segregation that may occur preferentially at such weak grain boundaries during high-energy irradiation [25–27]. In order to effectively apply RIDU to improve the resistance to radiation embrittlement in materials, it is important to elucidate the effects of pre-irradiation microstructures and irradiation conditions on RIDU and radiation embrittlement.

The behavior of radiation-enhanced precipitation and segregation at grain boundaries is expected to depend on the amount of TiC addition, grain size and dislocation density prior to irradiation. In this study, therefore, a fine-grained Mo alloy with a small amount of TiC addition, 0.2 wt%TiC, which is much smaller than that for MTC-10A, was fabricated by mechanical alloying (MA) and hot isostatic pressing (HIP). Then, specimens with high and low reduction rates in plastic working were prepared to introduce higher and lower dislocation densities prior to irradiation, designated as MTC-02H and MTC-02L, respectively. These specimens exhibited the lowest ductile-to-brittle transition temperature (DBTT) in the unirradiated state among the TiC dispersed Mo alloys developed so far [25,31]. MTC-02H and MTC-02L were irradiated with fast neutrons to 0.1 or 0.15 dpa with a controlled heat cycle (1 cycle or 4 cycle) at the similar temperatures to the case of MTC-10A in JMTR. The microstructure and mechanical properties of the irradiated specimens were examined.

2. Experimental

2.1. Specimens

Pure Mo (particle size: 5 μm, purity: 99.5%) and TiC (0.57 μm, 98%) powders were mixed to provide the target composition of Mo–0.2 wt%TiC under a glove box with a purified Ar atmosphere (99.99999% purity). The mixed powder and WC/Co balls were charged into two WC/Co milling containers having an inside volume of 250 cc. No lubricants were added to the powder for MA. Each container was sealed with an oxygen-free copper gasket, which prevented exposure to the air when MA was conducted outside the glove box. MA was conducted with a planetary ball mill (model: Fritsch P-5) for 360 ks in the purified Ar atmosphere. The MA processed powder was enclosed in a mild steel capsule (about 35 mm in diameter and 53 mm in height), which was TIG weld sealed after outgassing in a vacuum better than 1×10^{-6} Torr. The sealed capsule was HIPed at 1273 K and 196 MPa for 10.8 ks in an Ar atmosphere. The as-HIPed compact had the dimensions of approximately 25 mm in diameter and approximately 25 mm in height and a density of 10.12 g/cm^3, approximately 99.3% of theoretical, measured by the Archimedes' principle.

Table 1 shows the chemical composition, in wt ppm, of the as-HIPed compact, together with that for MTC-10A [25] for comparison. The contents of tungsten and cobalt arising from the milling containers and balls during MA were suppressed to 0.033 and 0.0017 wt%, respectively. The as-HIPed compact was cut into two pieces, which were mechanically polished to thicknesses of 9.4 mm and 13.8 mm (25 mm diameter). Each piece was hot forged and rolled around 1470 K and then cold rolled to 1.2 mm thick. The specimen thicknesses before and after each plastic working and the resultant reduction rates are listed in Table 2. Here, the reduction rates by hot forging and hot rolling for MTC-02L are controlled to be essentially the same as those for MTC-02H, respectively, whereas those by cold rolling are different: 29% for MTC-02L and 52% for MTC-02H. Specimens for TEM observations, X-ray diffraction

Table 1
Chemical compositions of MTC-02 and MTC-10A (wt ppm)

	Mo	Ti	C	O	N	W	Co	Fe	Ni	Cr	Ca	Cu	Mg	Si	Mn
MTC-02	Bal.	1500	490	960	144	330	17	35	21	19	11	5	11	56	2
MTC-10A	Bal.	7500	2270	1040	110	930	65	29	16	13	3	6	6	42	1

Table 2
Plastic working for MTC-02L and MTC-02H

	Initial thickness (mm)	Thickness after hot forging (mm)	Reduction rate by hot forging (%)	Thickness after hot rolling (mm)	Reduction rate by hot rolling (%)	Thickness after cold rolling (mm)	Reduction rate by cold rolling (%)
MTC-02L	9.4	2.5	73	1.7	32	1.2	29
MTC-02H	13.8	3.7	73	2.5	32	1.2	52

(XRD) analysis and Vickers microhardness and 3PB impact tests were prepared from the cold rolled sheets of MTC-02L and MTC-02H. The dimensions of the 3PB specimens were 1 mm by 1 mm by 20 mm, with the longitudinal direction parallel to the rolling direction. Thin foils for TEM were prepared by means of twin-jet electropolishing using a solution of 5 vol.% H_2SO_4 and 95 vol.% CH_3OH around 278 K at 20 V.

2.2. Neutron irradiation

Neutron irradiation was carried out using a controlled temperature capsule in JMTR. The irradiation conditions were (1) a fluence of 1.0×10^{24} n/m^2 ($E_n > 1$ MeV), which corresponds to 0.1 displacement per atom (dpa), with 1 cycle between 573 and 773 K (referred to as 1-cycle irradiation) and (2) a fluence of 1.5×10^{24} n/m^2, which corresponds to 0.15 dpa, with 4 cycles between 473 and 673 K (referred to as 4-cycle irradiation). The technical details of the controlled temperature-cycle irradiation was described elsewhere [32].

2.3. Evaluation of mechanical properties and microstructures

Vickers microhardness measurements were conducted at room temperature with a load of 1.96 N for 20 s. 3PB impact tests were carried out at temperatures from 150 to 473 K using a specially designed electrically controlled hydraulic machine with a span of 12.5 mm and an impact velocity of approximately 5 m/s [33]. Microstructural examinations were made by TEM with JEM-2000FX and JEM4000FX-II operating at 200 and 400 kV, respectively. XRD analysis was made to identify the dispersed particles with a voltage of 30 kV, amperage of 250 mA, a step angle of 0.02° and a counting time of 10 s/step.

3. Results and discussion

3.1. Mechanical properties

Fig. 1 shows the test temperature dependence of absorbed energy measured by 3PB impact tests for MTC-02H and MTC-02L, both in the unirradiated (as-rolled) and irradiated states. The absorbed energy (E_t) was normalized by Bt^2 to eliminate the effect of appreciable difference in specimen size (less than 15%) [25,31]. Here, B is the specimen width and t is the specimen thickness. The data points for the unirradiated MTC-02H and MTC-02L are lying on almost the same curve, whereas those for the irradiated ones shift to higher temperatures and are on different curves between MTC-02H and MTC-02L. Difference in irradiation cycle number also yields different test temperature dependence of E_t. The curves provide distinct transitions from ductile to brittle regions, namely DBTT's. DBTT was here defined as the temperature at which E_t is one half of the value at the upper shelf region. DBTT and its shift due to irradiation, i.e., ΔDBTT, are listed in Table 3. ΔDBTT due to the 1-cycle irradiation is slightly smaller in MTC-02H than in MTC-02L, while ΔDBTT due to the 4-cycle irradiation is significantly smaller in MTC-02L than in MTC-02H.

Fig. 2 shows the Vickers microhardness number, HV, in the as-rolled (unirradiated) and irradiated states for MTC-02L and MTC-02H. The values of HV in the as-rolled state are considerably lower in MTC-02L than in MTC-02H, reflecting difference in dislocation density between MTC-02H and MTC-02L. However, the increase in HV due to irradiation, ΔHV, namely radiation hardening, is distinctly larger in MTC-02L than in MTC-02H, regardless of irradiation cycle number (1-cycle or 4-cycle irradiation). This result agrees with the expectation from difference in sink site density,

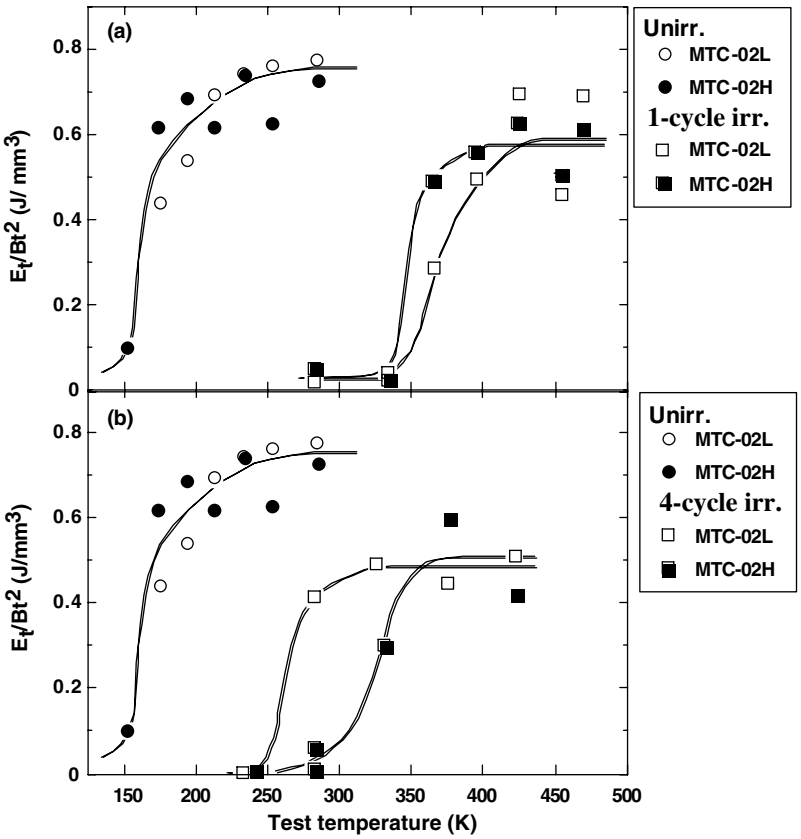

Fig. 1. Test temperature dependence of absorbed energy by 3PB impact tests before and after (a) 1-cycle irradiation and (b) 4-cycle irradiation in MTC-02L and MTC-02H.

Table 3
Summary of DBTT, ΔDBTT, HV and ΔHV for 1-cycle and 4-cycle irradiated specimens of MTC-02L and MTC-02H

	As-rolled DBTT (K)	1-cycle irr.		4-cycle irr.		As-rolled HV	1-cycle irr.		4-cycle irr.	
		DBTT (K)	ΔDBTT (K)	DBTT (K)	ΔDBTT(K)		HV	ΔHV	HV	ΔHV
MTC-02L	162	379	217	265	103	406	507	101	512	106
MTC-02H	162	349	187	319	157	462	528	66	511	49

i.e., dislocation density prior to irradiation, between MTC-02L and MTC-02H. The difference in ΔHV between the 1-cycle and 4-cycle irradiations for each of MTC-02L and MTC-02H is not very significant. The values of HV and ΔHV are listed in Table 3.

Fig. 3 shows a plot of ΔDBTT against ΔHV for MTC-02L and MTC-02H with the 1-cycle and 4-cycle irradiations. It is noteworthy that the 4-cycle irradiation results in a less degree of embrittlement than the 1-cycle irradiation for both MTC-02L and MTC-02H, although for the 4-cycle irradiation the irradiation temperature was lower by 100 K and the neutron fluence was 1.5 times higher than those for the 1-cycle irradiation in this investigation. The decrease in ΔDBTT from the 1-cycle to 4-cycle irradiation in MTC-02H corresponds to the decrease in ΔHV and can be explained from less radiation hardening. On the other hand, MTC-02L exhibits a significant decrease in ΔDBTT by approximately 100 K from the 1-cycle to 4-cycle irradiation in spite of a slight increase in ΔHV. This behavior of MTC-02L does not simply reflect radiation hardening and can be regarded as RIDU from the aspect of alleviation of radiation embrittlement in spite of increased radiation hardening. As described above, RIDU is attributable to strengthening of weak grain boundaries by radiation-enhanced precipitation and segregation.

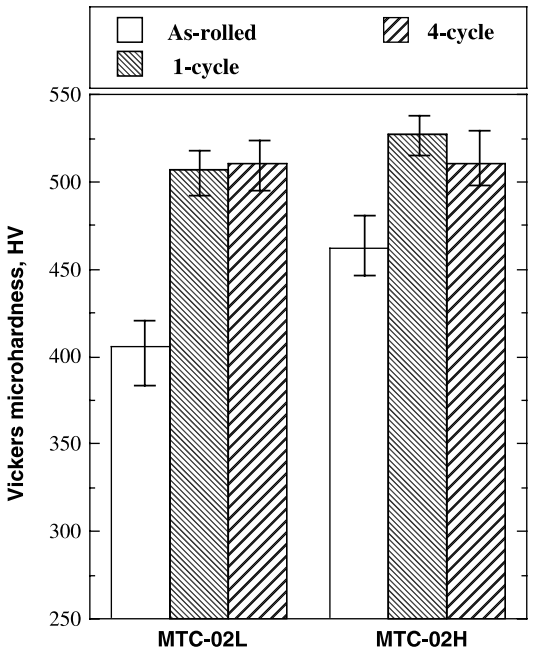

Fig. 2. Vickers microhardness, HV, for MTC-02L and MTC-02H before and after 1-cycle and 4-cycle irradiations.

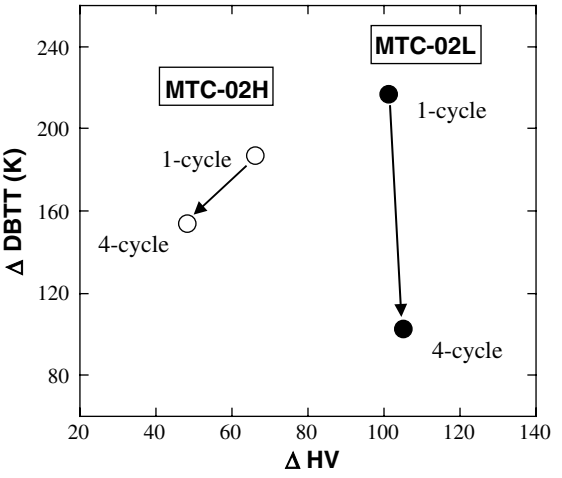

Fig. 3. Effects of irradiation conditions on radiation embrittlement, ΔDBTT, and radiation hardening, ΔHV, for MTC-02L and MTC-02H.

3.2. Microstructures

In order to examine the observed difference in the response of the properties to radiation between MTC-02H and MTC-02L, TEM observations on irradiation-produced defects and precipitation were made for MTC-02H and MTC-02L before and after the 4-cycle irradiation. Many small clusters and dislocation loops were observed for the irradiated specimens, but not for the unirradiated specimens. Fig. 4 shows an example of TEM dark field images of small clusters and dislocation loops for MTC-02L after the 4-cycle irradiation.

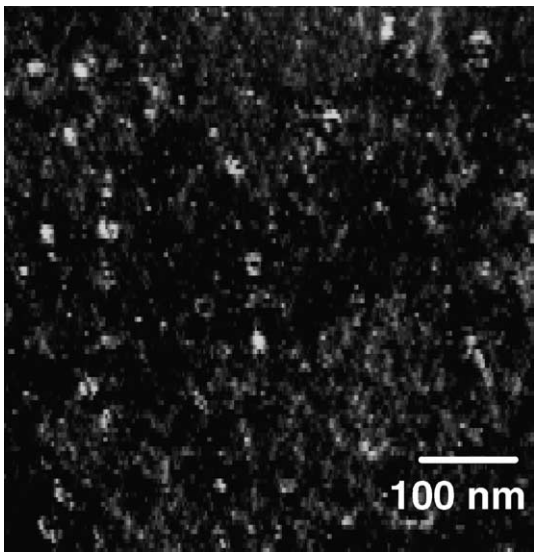

Fig. 4. TEM dark field image showing small clusters and dislocation loops in 4-cycle irradiated MTC-02L.

Fig. 5 shows size distributions of clusters/dislocation loops in MTC-02L and MTC-02H after the 4-cycle irradiation. The sizes are in a small range less than 10 nm, with an average diameter of 3.7 nm for MTC-02L and 3.4 nm for MTC-02H. On the other hand, significant difference was observed in the average number density of dislocation loops: 19.8×10^{21} m^{-3} for MTC-02L and 7.5×10^{21} m^{-3} for MTC-02H. Since such clusters/dislocation loops were not observed in the unirradiated state as mentioned above, the difference in the number density of clusters/dislocation loops may explain the difference in ΔHV between MTC-02L and MTC-02H after the 4-cycle irradiation.

Fig. 6 shows TEM bright field images of MTC-02L and MTC-02H after the 4-cycle irradiation, together with that of MTC-02L in the as-rolled state. It appears that the irradiation causes an increase in the amounts of large dispersoids, some of which have the similar size to the matrix grains.

Size distributions of the dispersoids are shown in Fig. 7, together with those in MTC-10A. It is obvious that the 4-cycle irradiation causes a shift of the size distribution to the larger side and significant increase in the average diameter of the dispersoids. In order to identify the substances of the dispersoids, EDX analysis was made and electron diffraction patterns were taken for relatively large dispersoids existing in the location almost free from the effect of the matrix, together with XRD analysis. The results are given in Figs. 8–10, showing

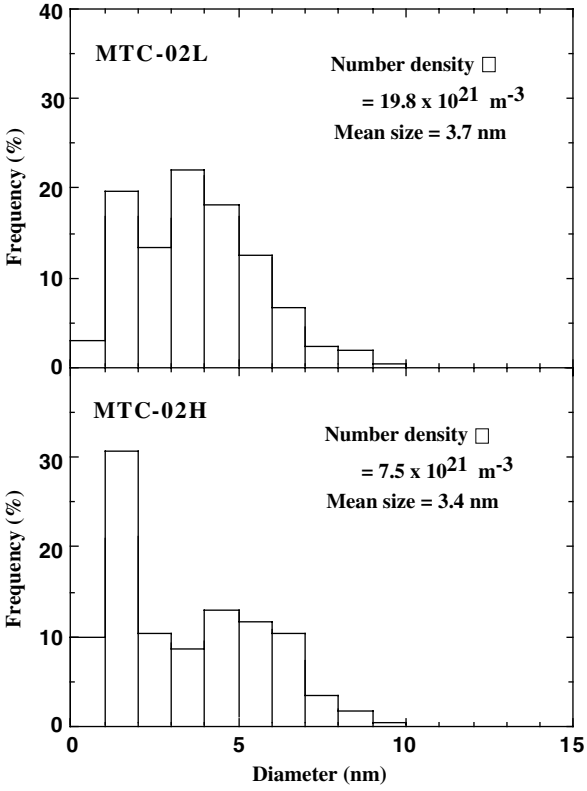

Fig. 5. Size distributions of the cluster/dislocation loops in MTC-02L and MTC-02H after 4-cycle irradiation.

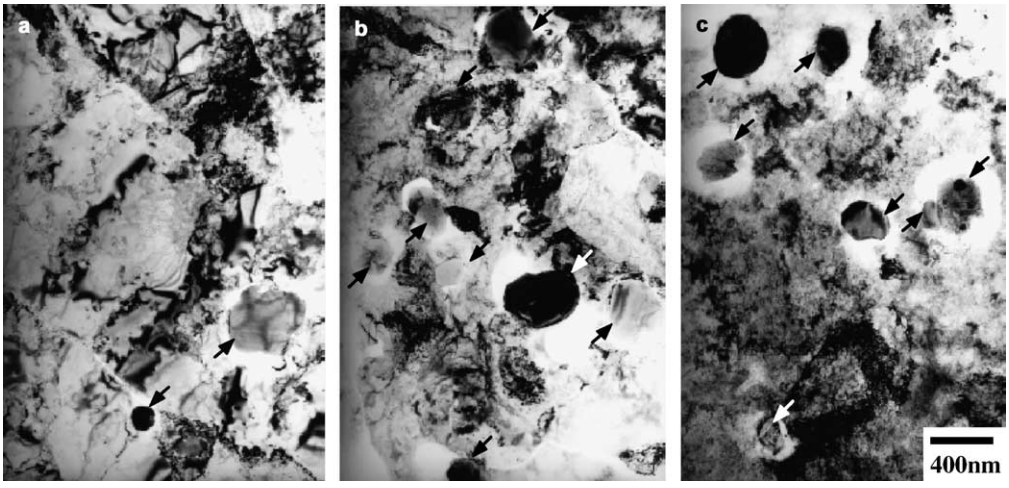

Fig. 6. TEM micrographs of (a) as-rolled MTC-02L, (b) 4-cycle irradiated MTC-02L and (c) 4-cycle irradiated MTC-02H. The arrows indicate large precipitates.

that the identified dispersoids are Mo_2C, $(Mo,Ti)_2C$, (Mo,Ti)C, (Ti,Mo)C and TiC, although they are not pure carbide, but contain appreciable amounts of oxygen and nitrogen [31]. It is seen from Fig. 10 that the sizes of TiC, (Ti,Mo)C and (Mo,Ti)C tend to be smaller than those of Mo_2C and $(Mo,Ti)_2C$, which may explain the result of Fig. 8.

Fig. 11 shows classification of the identified dispersoids for each of the above substances: dispersoids at grain boundaries and in the matrix. From Fig. 11, the

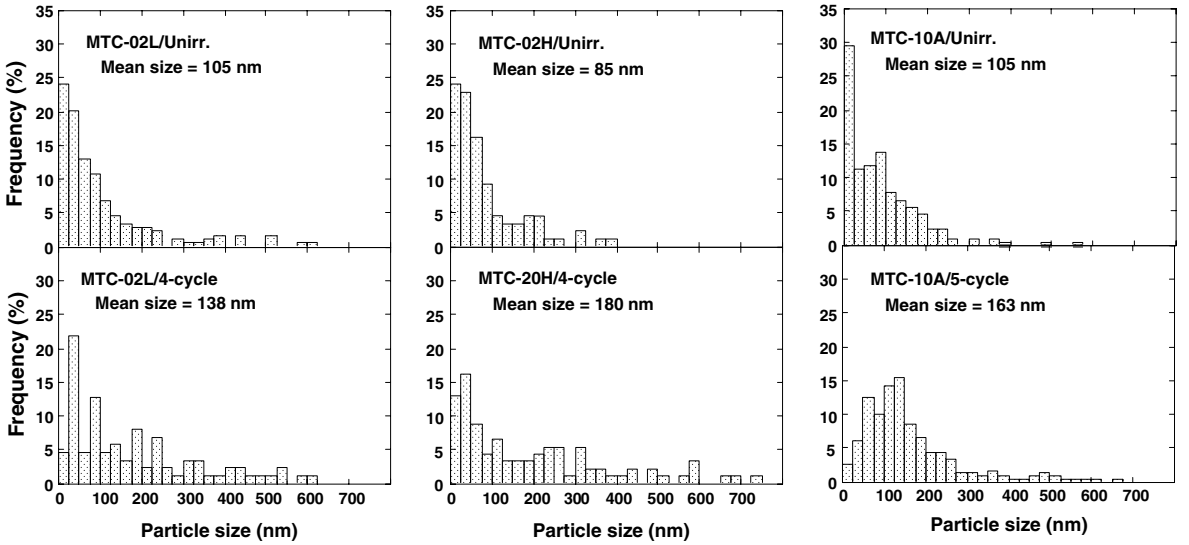

Fig. 7. Size distributions of each precipitate in MTC-02L and MTC-02H before and after 4-cycle irradiation, together with those in MTC-10A before and after 5-cycle irradiation.

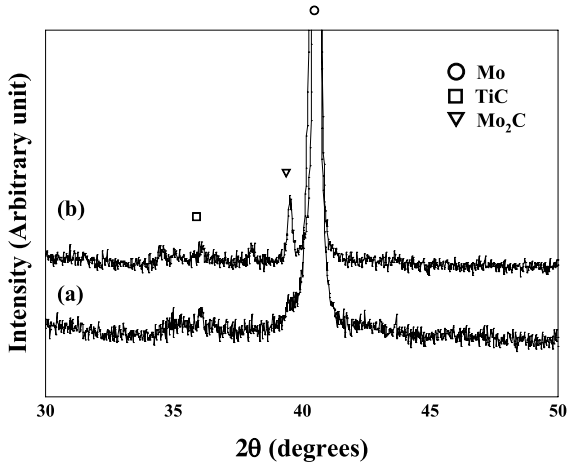

Fig. 8. X-ray diffraction patterns taken from MTC-02L (a) in the as-rolled state and (b) after 4-cycle irradiation.

ratio of the grain-boundary dispersoids to matrix dispersoids was estimated to be 0.41 for MTC-02H, 0.57 for MTC-02L and 0.60 for MTC-10A. It is reported that $(Mo,Ti)_2C$, (Mo,Ti)C, (Ti,Mo)C and TiC have a beneficial effect of strengthening weak, high-energy grain boundaries acting as a crack initiator in Mo by replacing weak grain boundaries with stronger interfaces [28,30,34]. Grain-boundary dispersoids are presumed to preferentially form at such weak, high-energy grain boundaries. We assume that the proportion of weak, high-energy grain boundaries to the total grain boundaries is the same among MTC-10A, MTC-02L and MTC-02H because these alloys were prepared by the identical procedure and have almost the same grain size. Then, it is reasonable to say that the strengthening of the weak, high-energy grain boundaries by dispersoids were more significant in MTC-10A and MTC-02L than in MTC-02H, and thereby MTC-10A and MTC-02L showed higher resistance to radiation embrittlement than MTC-02H. The observed difference in the proportion of grain-boundary dispersoids between MTC-10A, MTC-02L and MTC-02H may be explained as follows.

It is well known that grain boundaries and dislocations are effective sites for heterogeneous nucleation of precipitation. MTC-02H contains a higher density of dislocations prior to irradiation than MTC-02L, owing to a high reduction rate. As a result, heterogeneous precipitation at dislocations may occur more intensively for MTC-02H than for MTC-02L. The amounts of the constituents of the dispersoids, such as carbon, oxygen and nitrogen, are essentially the same for MTC-02L and MTC-02H. This implies that promotion of precipitation at dislocations suppresses precipitation at grain boundaries. It is thus likely that MTC-02H exhibits less precipitation at grain boundaries than MTC-02L. In the case of MTC-10A, on the other hand, 1.0%TiC was added and thus the content of carbon, an important constituent of the dispersoids, is five times higher than in MTC-02L and MTC-02H. A sufficient addition of TiC resulted in the increased amount of grain-boundary dispersoids.

3.3. Radiation-induced ductilization

Even in the specimen with only 0.2%TiC addition, tendency of RIDU was observed for the 4-cycle

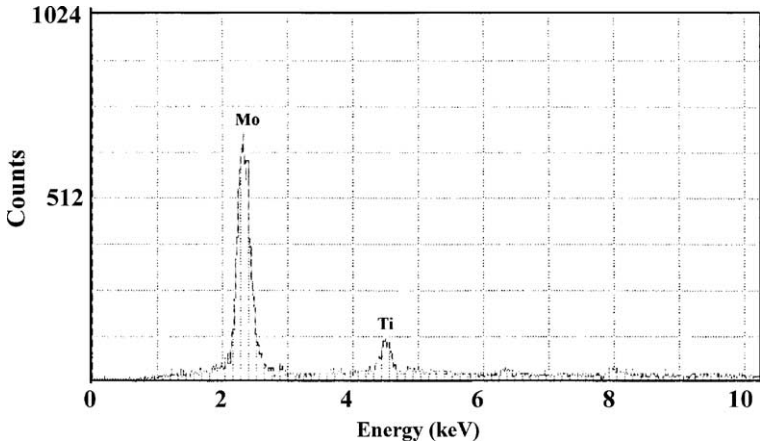

Fig. 9. EDX spectrum for a large precipitate with a diameter of approximately 300 nm. The precipitate exists in the location almost free from the effect of matrix.

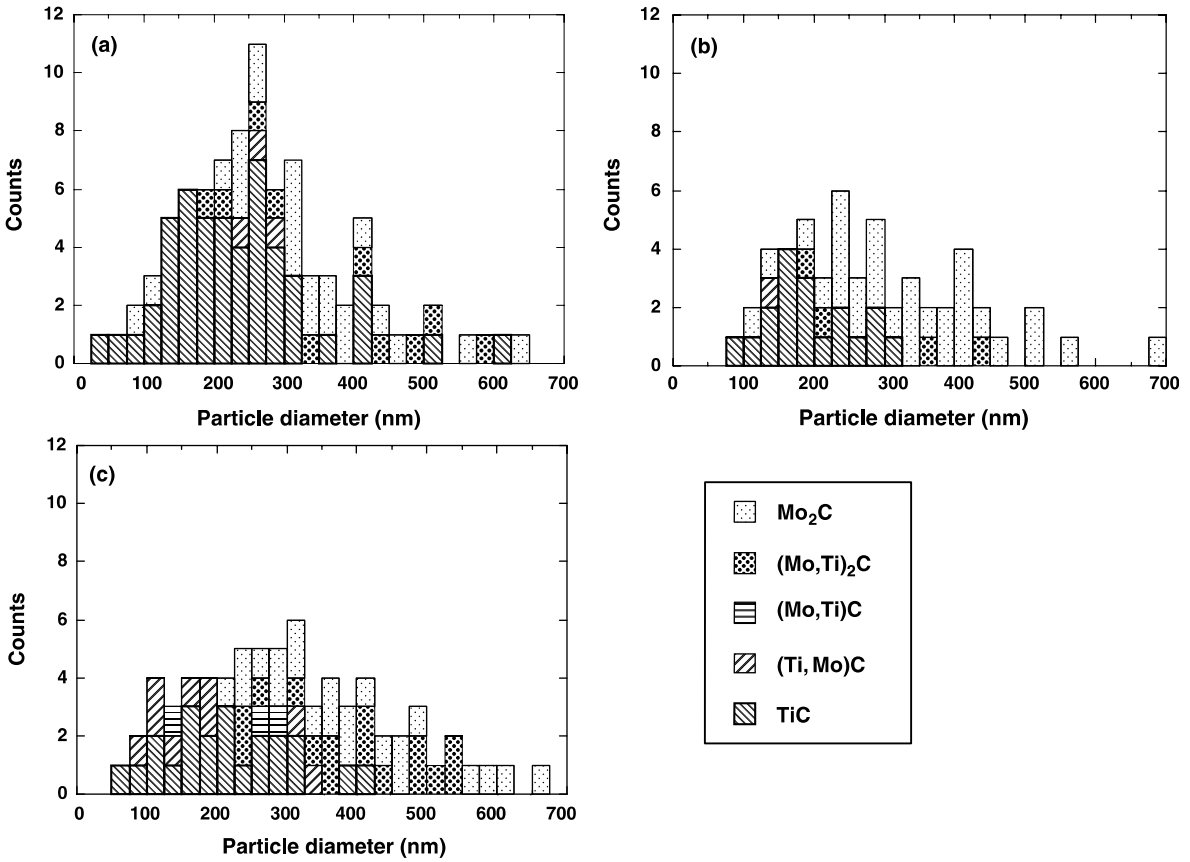

Fig. 10. Size distributions of each of the identified precipitates in 4-cycle irradiated (a) MTC-02L and (b) MTC-02H and (c) 5-cycle irradiated MTC-10A.

irradiation, but not for the 1-cycle irradiation. This indicates that the irradiation condition is another important factor for the occurrence of RIDU or radiation embrittlement. The significance of the 4-cycle irradiation between 473 and 673 K is discussed below.

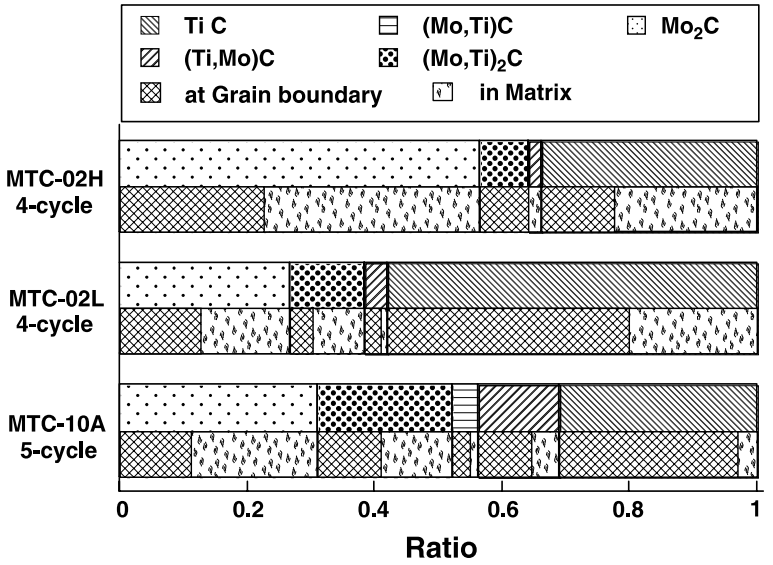

Fig. 11. Ratio of dispersoids existing at grain boundaries to those in matrix for each of the identified dispersoids for irradiated MTC-02L, MTC-02H and MTC-10A.

High-energy neutron irradiation is known to cause cascades, which lead to depleted zones, isolated self interstitial atoms (SIA) and vacancies. At the lower temperature of 473 K SIAs can move, but vacancies are difficult to move. Therefore, during 473 K irradiation SIAs move to sink sites and/or aggregate to form clusters and dislocation loops, and depleted zones, which are regarded as vacancy clusters, and isolated vacancies are accumulated in the matrix, although some of them act as sink sites for mobile SIAs. Since the irradiation temperature in the final heat cycle before switching off the heating current for the 4-cycle irradiation was 473 K, the observed dislocation loops are likely of the interstitial type. Accordingly, each irradiation at 473 K during the 4-cycle irradiation may leave a high density of isolated vacancies and small clusters of vacancies, in addition to a high density of interstitial loops.

When the irradiation temperature is increased from 473 K to 673 K where vacancies become mobile, the accumulated, isolated vacancies can begin to move almost simultaneously and may enhance precipitation at grain boundaries and dislocations. The grain boundaries and dislocations provide short circuit diffusion paths, and the dispersoids formed at grain boundaries and dislocations can easily grow. A high density of grain boundaries (fine grains) and dislocations prior to irradiation in the specimens used in this study are likely responsible for the observed large dispersoids. As the cycle number increases, the number and size of dispersoids at grain boundaries and dislocations increase. The amount ratio of the dispersoids at grain boundaries to those in the matrix depends on grain size relative to dislocation density prior to irradiation. As the grain size and/or dislocation density decrease, the contribution of grain-boundary dispersoids to the occurrence of RIDU becomes more significant.

In addition, grain size refinement has the beneficial effects of decreasing both the effective size of weak grain boundaries and their proportion to the total grain boundaries, leading to reduction in the amount of grain boundary dispersoids required to strengthen weak grain boundaries. The post-irradiation properties of Mo are hence greatly influenced by microstructural parameters: the amount of TiC addition, dislocation density prior to irradiation and grain size. These parameters are responsible for the occurrence of RIDU or radiation embrittlement. In other words, it is possible to relieve radiation embrittlement or even produce RIDU in Mo by controlling these parameters.

4. Conclusions

In order to clarify the effect of pre-irradiation microstructures and irradiation conditions on radiation embrittlement or radiation-induced ductilization (RIDU), fine-grained Mo–0.2 wt%TiC specimens with high and low reduction rates, designated as MTC-02H and MTC-02L, respectively, were prepared by mechanical alloying and HIP, followed by plastic working. They were irradiated with fast neutrons to 0.1 or 0.15 dpa with 1 cycle or 4 cycles between 573 and 773 K, and 473 and 673 K, respectively, in JMTR. Vickers microhardness and 3PB impact tests and TEM microstructural observations were performed. The main results obtained are as follows:

1. The degree of radiation embrittlement, assessed by DBTT shifts due to irradiation, depends strongly on the density of dislocations prior to irradiation and irradiation cycle number.
2. The 4-cycle irradiation suppresses radiation embrittlement of MTC-02H and MTC-02L compared with the 1-cycle irradiation, in spite of a lower irradiation temperature and 1.5 times higher neutron fluence than those for the 1-cycle irradiation.
3. The suppression in radiation embrittlement by the 4-cycle irradiation is much more significant in MTC-02L than in MTC-02H. The significant suppression in MTC-02L ($\Delta DBTT = -114$ K) occurs in spite of a slight increase in radiation hardening. This behavior of MTC-02L can be regarded as RIDU.
4. Many small clusters and dislocation loops are formed in the 4-cycle irradiated MTC-02H and MTC-02L, with average diameters of 3.4 and 3.7 nm, respectively. The number density of dislocation loops is much higher in MTC-02L than in MTC-02H. This result is due to the difference in sink (dislocation) density, and these dislocation loops are presumed to be of the interstitial type.
5. Dispersoids with a considerably larger average size than those in the unirradiated specimens are formed at grain boundaries and in the matrix after the 4-cycle irradiation. They are identified to be Mo_2C, $(Mo,Ti)_2C$, (Mo,Ti)C, (Ti,Mo)C and TiC, although they are not pure carbide, but contain appreciable amounts of oxygen and nitrogen.
6. The fraction of the dispersoids existing at grain boundaries is larger in MTC-02L than in MTC-02H. This precipitation behavior is attributed to a lower dislocation density in MTC-02L than in MTC-02H. The strengthening effect of weak grain boundaries by the dispersoids is hence larger in MTC-02L than in MTC-02H.
7. The grain size and dislocation density prior to irradiation, amount of TiC addition and irradiation conditions are the crucial factors for RIDU or radiation embrittlement. In order to suppress radiation embrittlement in Mo, it is important to control such amount of TiC addition, grain size and dislocation density prior to irradiation.

Acknowledgements

The authors would like to express their gratitude to Drs Y. Aono and R. Ishibashi, Hitachi Research laboratory, Hitachi, Ltd., for their help with use of HIP apparatus, and to Dr S. Matsuo for his review of the paper. The present work was supported by Grant-in-Aid for Scientific Research (A) (#13308022), Japan Society for the Promotion of Science, which is greatly appreciated.

References

[1] J.M. Steichen, J. Nucl. Mater. 60 (1976) 13.
[2] B.L. Cox, F.W. Wiffen, J. Nucl. Mater. 85&86 (1979) 901.
[3] K. Abe, T. Takeuchi, M. Kikuchi, S. Morozumi, J. Nucl. Mater. 99 (1981) 25.
[4] S. Morozumi, K. Abe, M. Kikuchi, M. Hasegawa, J. Nucl. Mater. 108&109 (1982) 417.
[5] F.W. Wiffen, in: R.H. Cooper, E.E. Hoffman (Eds.), Proc. Symposium on Refractory Alloy Technology for Space Nuclear Power Applications, 1984, p. 252.
[6] K. Abe, M. Kikuchi, K. Take, S. Morozumi, J. Nucl. Mater. 122&123 (1984) 671.
[7] Y. Hiraoka, M. Okada, T. Fujii, M. Tanaka, A. Hishinuma, J. Nucl. Mater. 141–143 (1986) 837.
[8] F. Morito, K. Shiraishi, J. Nucl. Mater. 179–181 (1991) 592.
[9] K. Abe, F. Nagae, S. Morozumi, J. Nucl. Mater. 179–181 (1991) 1088.
[10] I.V. Gorynin, V.A. Iganatov, V.V. Rybin, S.A. Fabritsiev, V.A. Kazakov, V.P. Chakin, V.A. Tsykanov, V.R. Barabash, Y.G. Prokofyev, J. Nucl. Mater. 191–194 (1992) 421.
[11] S.A. Fabritsiev, V.A. Go sudarenkova, V.A. Potapova, V.V. Rybin, L.S. Kosachev, V.P. Chakin, A.S. Pokrovsky, V.R. Barabash, J. Nucl. Mater. 191–194 (1992) 426.
[12] G.V. Muller, D. Gavillet, M. Victoria, J.L. Martin, J. Nucl. Mater. 212–215 (1994) 1283.
[13] B.N. Singh, A. Horsewell, P. Toft, J.H. Evans, J. Nucl. Mater. 212–215 (1994) 1292.
[14] B.N. Singh, J.H. Evans, A. Horsewell, P. Toft, D.J. Edwards, J. Nucl. Mater. 223 (1995) 95.
[15] A. Hasegawa, K. Abe, M. Satou, K. Ueda, C. Namba, J. Nucl. Mater. 225 (1995) 259.
[16] A. Hasegawa, K. Abe, M. Satou, C. Namba, J. Nucl. Mater. 233–237 (1996) 565.
[17] V. Chakin, V. Kazakov, J. Nucl. Mater. 233–237 (1996) 570.
[18] K. Watanabe, A. Hishinuma, Y. Hiraoka, T. Fujii, J. Nucl. Mater. 258–263 (1998) 848.
[19] B.N. Singh, J.H. Evans, A. Horsewell, P. Toft, G.V. Muller, J. Nucl. Mater. 258–263 (1998) 865.
[20] V.P. Chakin, F. Morito, V.A. Kazakov, Yu.D. Goncharenko, Z.E. Ostrovsky, J. Nucl. Mater. 258–263 (1998) 883.
[21] A. Hasegawa, K. Ueda, M. Satoh, K. Abe, J. Nucl. Mater. 258–263 (1998) 902.
[22] M. Scibetta, R. Chaouadi, J.L. Puzzolante, J. Nucl. Mater. 283–287 (2000) 455.
[23] Y. Nemoto, A. Hasegawa, M. Satou, K. Abe, Y. Hiraoka, J. Nucl. Mater. 324 (2004) 62.
[24] B.V. Cockeram, J.L. Hollenbeck, L.L. Snead, J. Nucl. Mater. 324 (2004) 77.
[25] Y. Kitsunai, H. Kurishita, T. Shibayama, M. Narui, H. Kayano, Y. Hiraoka, J. Nucl. Mater. 239 (1996) 253.

[26] H. Kurishita, Y. Kitsunai, T. Kuwabara, M. Hasegawa, Y. Hiraoka, T. Takida, T. Igarashi, J. Plasma Fus. Res. 75 (1999) 594.
[27] H. Kurishita, Basic Studies in the Field of High-Temperature Engineering, OECD, 2002, p. 103.
[28] A. Kumar, E.L. Eyre, Proc. R. Soc. Lond. A370 (1980) 431.
[29] J.B. Brosse, R. Fillit, M. Biscondi, Scr. Metall. 15 (1981) 619.
[30] H. Kurishita, H. Yoshinaga, Mater. Forum 30 (1989) 161.
[31] H. Kurishita, Y. Kitsunai, T. Shibayama, H. Kayano, Y. Hiraoka, J. Nucl. Mater. 233–237 (1996) 557.
[32] M. Narui, H. Kurishita, H. Kayano, T. Sagawa, N. Yoshida, M. Kiritani, J. Nucl. Mater. 212–215 (1994) 1665.
[33] H. Kayano, H. Kurishita, M. Narui, M. Yamazaki, Ann. Chim. Fr. 16 (1991) 309.
[34] H. Kurishita, M. Asayama, O. Tokunaga, H. Yoshinaga, Mater. Trans. JIM 30 (1989) 1009.